

# department of electrical engineering



CR 114392

THE FEASIBILITY OF  
ELECTROHYDRODYNAMIC HEAT PIPES

Research Report #1

October, 1971

by T. B. Jones

NASA Grant # NGR-06-002-127

Reproduced by  
NATIONAL TECHNICAL  
INFORMATION SERVICE  
Springfield, Va. 22151

prepared for  
Ames Research Center  
National Aeronautics and Space Administration  
Moffett Field, California 93405



N72-13914 (NASA-CR-114392) THE FEASIBILITY OF  
ELECTROHYDRODYNAMIC HEAT PIPES T.B. Jones  
(Colorado State Univ.) Oct. 1971 61 p  
CSCL 20M

Unclas  
10657

G3/33

This work was performed under the  
auspices of NASA/Ames Research Center,  
Grant # NGR-06-002-127. Mr. J. P.  
Kirkpatrick is the Technical Monitor.

The research program is being conducted  
by Dr. Thomas B. Jones, Assistant  
Professor of Electrical Engineering,  
Colorado State University, Ft. Collins,  
Colorado 80521.

THE FEASIBILITY OF  
ELECTROHYDRODYNAMIC HEAT PIPES

Research Report #1

October, 1971

by T. B. Jones

Department of Electrical Engineering

Colorado State University

Ft. Collins, Colorado 80521

NASA Grant # NGR-06-002-127

prepared for

Ames Research Center

National Aeronautics and Space Administration

Moffett Field, California 93405

## TABLE OF CONTENTS

I.	Introduction . . . . .	1
II.	Summary of Research Tasks . . . . .	3
	A. Theory of Operation . . . . .	3
	Flow Dynamics . . . . .	3
	Heat Transfer . . . . .	4
	Operational Limits . . . . .	4
	B. Design Criteria . . . . .	4
	C. Evaluation of Optional Design Features . . . . .	5
III.	EHD Heat Pipe Theory . . . . .	6
	A. The Analogy . . . . .	6
	B. Flow Dynamics . . . . .	12
	The Dielectric Pumping Head . . . . .	12
	Viscous Head Losses . . . . .	16
	Momentum Effects on Vapor Flow . . . . .	18
	Vapor Shear Forces . . . . .	18
	Summary . . . . .	19
	C. Heat Transfer in EHD Heat Pipes . . . . .	19
	Conduction Heat Transfer . . . . .	20
	Vapor Expansion . . . . .	20
	Evaporation Heat Transfer . . . . .	21
	Condensation Heat Transfer . . . . .	24
	Threaded Groove Heat Transfer . . . . .	26
	D. Entrainment . . . . .	28
	E. EHD Wavespeed Limit . . . . .	29
IV.	Rudiments of the Design of EHD Heat Pipes . . . . .	30
	A. Fluid Data . . . . .	30
	Classification . . . . .	30
	EHD Fluid Transport Factor . . . . .	31
	The Wicking Height . . . . .	31
	Summary . . . . .	33
	B. EHD Heat Pipe Optimization . . . . .	33
	The Optimization Procedure . . . . .	35
	System Constraints . . . . .	36
V.	Summary . . . . .	40
	The Wicking Limit . . . . .	40
	Priming and Startup . . . . .	41
	Susceptibility to Boiling . . . . .	41
	Condensation . . . . .	42
	Heat Pipe Control . . . . .	42
	Some Optional Design Features . . . . .	43
	Conclusion . . . . .	44

APPENDICES

A. Performance Calculations for Optimized EHD Heat Pipes . . . . .	45
B. Nomenclature . . . . .	51
References . . . . .	53

LIST OF TABLES

I.	Dielectric Height of Rise and Vapor Breakdown Strength of a few Liquids . . . . .	8
II.	Peak Nucleate Pool Boiling Heat Flux and approximate Superheat Values . . . . .	24
III.	Useful Working Dielectric Fluid Properties - Classification . . . . .	30
IV.	Properties of Selected Dielectric Heat Transfer Fluids . . . . .	34

## LIST OF FIGURES

1.	A Demonstration of the Polarization Electrohydrodynamic Force on a Dielectric Fluid . . . . .	7
2.	A Two-Dimensional Representation of a Capillary Wick, showing Vertical Profile. . . . .	11
3.	Prototype EHD Heat Pipe Using Parallel-Plate Flow Structures . . . . .	13
4.	Possible EHD Heat Pipe Utilizing Dielectric "Tent" Flow Structures . . . . .	14
5.	Typical Boiling Heat Transfer Curve, with and without Gradient Electric Field Enhancement . . . . .	22
6.	EHD Transport Factor for Various Dielectric Liquids . . . . .	32
7.	Available Height of Rise for Various Dielectric Liquids . . . . .	32
8.	Theoretical Operational Limits of EHD Heat Pipe in (s, V) Space . . . . .	37
A1.	Theoretical Maximized Thermal Throughput versus $N_{EHD}$ for several EHD Heat Pipes . . . . .	46

## I. Introduction

This research program was undertaken to study the feasibility of an electrohydrodynamic (EHD) heat pipe. Though EHD effects encompass a rather large number of interesting and potentially useful phenomena, the primary effort here has been directed at utilizing the well-known effect which a non-uniform electrostatic field exerts upon insulating dielectric liquids. This effect is, specifically, the tendency of dielectric liquids to be collected and held in hydrostatic equilibrium in regions of higher electric field intensity. To the author's knowledge, there has been only one other significant proposal regarding the implementation of electric field effects in a heat pipe. This is the suggestion of Abu-Romia to use electrocapillarity to aid in the flow of liquid through a capillary wick.<sup>1</sup> The present scheme differs markedly from the electrocapillary system in that the capillary wick structure is completely removed and replaced by an electrode structure in an EHD heat pipe.

A useful and instructive background exists in the proposed implementation of the polarization force for the management of dielectric liquids. Workers have studied various schemes for the control of propellant liquids in spacecraft by the placement of electrode structures in propellant tanks.<sup>2, 3, 4</sup> The electrode structure can be designed to minimize sloshing, thus insuring the presence of fuel at the drain during rocket firing. Approximately 100% propellant drainage, quite important in spacecraft, can also be attained.

Actually, the sub-field of electrohydrodynamic heat transfer has existed for some time, but the main emphasis has been on the basic processes of convective<sup>5</sup>, boiling,<sup>6-9</sup> and condensation<sup>10-12</sup> heat transfer as augmented by electric field effects. The possible application of these

effects to spacecraft heat transfer problems has been considered.<sup>13</sup> But, curiously, it has been only quite recently suggested that the application of EHD to the rapidly developing technology of heat pipes be seriously studied. In particular, Jones has proposed an EHD heat pipe which replaces the wick of a conventional capillary heat pipe with an electrode structure.<sup>14</sup> An initial promise of this scheme, which Jones recognized, is the effective elimination of the so-called wicking limit imposed on many moderate and low-temperature heat pipes (using cryogenic or organic liquids and homogeneous wicks<sup>15</sup>). This first research report presents the results obtained to date in a study undertaken to explore the feasibility of the electrohydrodynamic heat pipe concept.

## II. Summary of Research Tasks

For the purposes of reviewing the major sections of the program, the work has been divided into three research tasks involving: theory of operation; design criteria; and evaluation of optional design features. Further subdivision and definition of the work is summarized in this section.

### A. Theory of Operation

The operation of an EHD heat pipe is in many respects analogous to that of "conventional" capillary devices, a viewpoint fully exploited in the development of the theory of section III. However, the presence of a free dielectric liquid surface in a non-uniform electric field produces some profound effects on the operation of an EHD heat pipe, effects which have no analogous behavior in capillary devices. The thrust of the effort has thus far been in the areas of flow dynamics, heat transfer (evaporation and condensation), and device limitations (e.g., entrainment, sonic limit, etc.).

#### Flow Dynamics

The steady flow equations are easily developed, based upon a balance of liquid and vapor viscous losses with the available electric "pumping" pressure head. A limited understanding of Maxwell electric surface stresses is useful, but the extent of the analogy to capillary "pumping" simplifies the theory considerably. Of interest is the point that transitional or even turbulent liquid flow is predicted for EHD heat pipe operation. Whether or not true turbulent flow is ultimately attainable in such heat pipes must await further study and perhaps experimental effort. The possible importance of large shear stresses, exerted on the liquid free

surface by the high speed vapor flow, is a factor which complicates the flow dynamics further.

### Heat Transfer

The principal heat transfer problems in any heat pipe are the evaporation (or possibly boiling) and the condensation which occur respectively at the "hot" and "cold" ends of the device. As stated in section I, these processes can be significantly enhanced when electric fields are present. The purpose of section III.C. is to explore the ramifications of EHD heat transfer for EHD heat pipes in qualitative and (when possible) quantitative terms.

### Operational Limits

Based on the theoretical model of EHD heat pipes, a number of limiting constraints on their performance may be drawn. Some of these constraints are familiar by analogy to capillary devices, while others are new. They include: the fundamental "pumping" limit (basically analogous to the wicking limit of conventional heat pipes); evaporation and condensation heat transfer limits; entrainment (analogous); sonic (the same as in conventional heat pipes); the EHD wavespeed limit (no analogy); electrical breakdown (no analogy). This list presents the important presently-recognized constraints on EHD heat pipe operation.

### B. Design Criteria

Taking into account the theory and operational limits which result from the modeling, it is appropriate to develop design procedures which will give optimized performance for EHD heat pipes. The performance predictions can then be compared to data on existing conventional heat

pipes to assess the relative merits of the two schemes.\* One aspect of the design procedure is the selection of working dielectric fluids. Section IV.A defines important selection criteria and introduces an EHD liquid transport factor, which measures the relative merits of candidate working fluids.

The most difficult aspect of the design procedure involves the optimization of EHD heat pipe performance by proper selection of operating voltage, electrode configuration and dimensions, and operating pressure. This can only be done with complete knowledge of the operational constraints. As a first cut at the problem, a simple optimization based on a minimum flow resistance criterion has been performed. Though this criterion is not the best choice,<sup>16</sup> it is an easy one to use and produces results from which performance parameters for some rather high heat capacity EHD devices can be gleaned. A more valuable optimization, based on the criterion of maximized effective thermal conductance, must be delayed until EHD enhanced evaporation and condensation are more thoroughly understood.

#### C. Evaluation of Optional Design Features

A number of options exist in the use of electrohydrodynamic effects, and some thought has been given to their implementation into working capillary heat pipes, as well as EHD devices. These are discussed in the conclusion, section V.

-----

\* The greater complexity of EHD heat pipes will clearly have to be offset by a set of distinct advantages in order to justify their development past the initial stages.

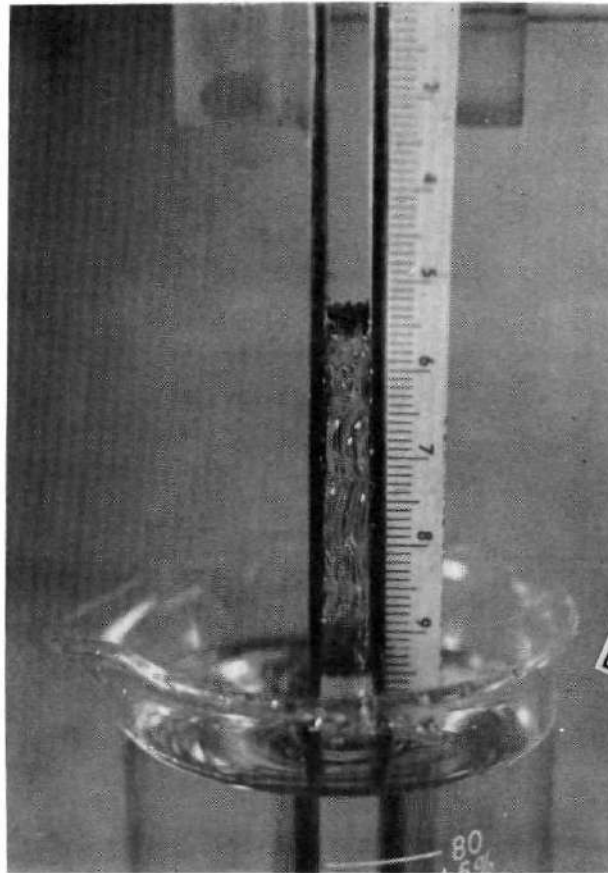
### III. EHD Heat Pipe Theory

#### A. The Analogy

It is easiest to develop the useful analogy between capillary and EHD heat pipe theory by first discussing a simple experiment which provides the classic illustration of the polarization force. Figure 1 shows a pair of long, thin parallel electrode plates, spaced approximately 0.5 centimeters apart, and dipped into a dielectric liquid (in this case, Mazola Corn Oil with a relative dielectric constant of  $\epsilon \sim 3.1$ ). The plates are held at a potential difference of  $\sim 24$  KV-rms. In response to the polarization force, the liquid rises between the plates; we see that at 24 KV-rms, this height of rise,  $h$ , is on the order of five centimeters. (Note that the experiment is carried out in an atmosphere of dry  $N_2$  gas at  $\sim 400$  psi. The high pressure is used to guard against corona and electrical breakdown of the air or vapor. Alternating voltage at 400 Hz insures the absence of free surface charge, which would disrupt static equilibrium. The ripples plainly visible on the free liquid surface are associated with a parametric effect of no interest here.)

This "electrohydrostatic" equilibrium problem has been analyzed by Jones (among others), who has determined the vertical liquid profile.<sup>14</sup> Figure 1 does not show it clearly, but observation indicates that the liquid bulges out from between the plates, more toward the bottom and less toward the top. The Maxwell stress tensor<sup>17</sup> may be used to calculate  $h$ , the height to which the liquid will rise,<sup>14</sup> as a function of applied electric field.

$$h \approx \frac{(\epsilon_l - \epsilon_o) E^2}{2\rho_l g_o} \quad , \quad (1)$$



Reproduced from  
best available copy.

Figure 1. A Demonstration of the Polarization Electrohydrodynamic force on a Dielectric Fluid  
( $V = 24 \text{ KV-rms}$ ,  $s \approx 0.5 \text{ cm}$ ).

where:  $\epsilon_l$  = liquid dielectric constant,  
 $\epsilon_0 = 8.85 \cdot 10^{-12} \frac{\text{farads}}{\text{meter}}$  (permittivity of free space),  
 $E \approx V/s$  (electric field between plates),  
 $V$  = rms voltage,  
 $s$  = electrode spacing,  
 $\rho_l$  = liquid density,  
 $g_0 = 9.81 \frac{\text{meters}}{\text{sec}^2}$  (earth gravitational acceleration),

and in Equation (1) the vapor density has been neglected. (Refer to Appendix B for a complete list of all notations.) Relevant to EHD heat pipe operation in terrestrial applications is the maximum height to which a

fluid	$h_{\text{max}}$ (cm)	$E_b$ (KV/cm)	@ $T_b$ (°F)
Freon-113	9.8	156.	118
Freon-12	3.0	93.5	-22
Freon E-3	18.9	194.	306
Dowtherm A #	~48.0	~200.	495
CP-9 * (Monsanto)	~19.	~195.	567
FC-43 (3M)	> 8.3	> 138.	345

# estimated vapor breakdown strength

\* incomplete data on fluid vapor properties

Table I. Dielectric Height of Rise and Vapor Breakdown Strength of a Few Liquids at Atmospheric Boiling Point

dielectric liquid can be raised by an electric field. This may be determined by using the breakdown field strength of the vapor in Eq. (1).

Table I contains such data for a few useful fluids. (Note that the atmospheric pressure breakdown strength is used.) At somewhat elevated pressures on the order of two to three atmospheres, the breakdown strength improves significantly, resulting in large increases in the maximum height of rise,  $h$ .

It is harder to explain where the polarization force is acting than merely to introduce the Maxwell stress tensor and describe the effective pressure differences across the liquid interface. In our case with a purely tangential electric field and no free surface charge, the stress is purely normal, and accounts only for a pressure difference. The electrical surface traction at a surface "1" is

$$T_n^e = \frac{(\epsilon_l - \epsilon_0) E_1^2}{2} \quad (2)$$

and it acts outward from the liquid surface into the vapor region. For overall surface force balance, this requires that the pressure in the liquid be less than ambient.

$$p_{\text{liquid}} - p_{\text{vapor}} + T_n^e = 0 \quad (3)$$

Because the internal liquid pressure  $p_{\text{liquid}}$  must increase downward due to the gravitational body force  $\rho_l g_0$ ,  $T_n^e$  must decrease downward to satisfy (3) everywhere. This balance is accomplished by the liquid bulging out further into the electrical fringing field region at the bottom than at the top. This is experimentally observed, though Figure 1 does not show it. Thus,

an essential non-uniformity in the electric field, achieved in the fringing region, is crucial to the hydrostatic profile.

At this point, an analogy between a capillary wick structure and an electrode structure begins to emerge. A wick, dipped into a liquid, will allow the rise of the liquid to a height determined by the surface tension and wetting properties of the liquid and the pore size of the wick. The height of rise  $h_{cap}$  is well-known to be:

$$h_{cap} = \frac{2\gamma \cos \theta}{R\rho_l g_0} \quad (4)$$

where  $\gamma$  = surface tension,

$\theta$  = wetting angle

$R = 2 \left( \frac{1}{r_1} + \frac{1}{r_2} \right)^{-1}$ , effective radius of curvature at the uppermost wetted part of the wick.

R can often be approximated as the effective pore size of the wicking material. Figure 2 shows the somewhat idealized vertical profile of the wick structure. Note that the liquid "bulges" further out into the vapor space near the bottom than at the top. This is effected by an increase in the radius of curvature R going downward.

The comparison of these two hydrostatic configurations has uncovered the basis for the promised analogy. Upon application of heat to the top section of the electrode structure in Figure 1, or the wick structure in Figure 2, liquid will evaporate, the interface will recede into the structure, and more liquid will move up to replace it, due to hydrostatic force imbalance. These are the effective "pumping" mechanisms of, respectively, EHD and capillary structures. The electrodes are capable both of orienting static fluid and guiding it if the fluid flows. This is just the function of the wick in capillary heat pipes.

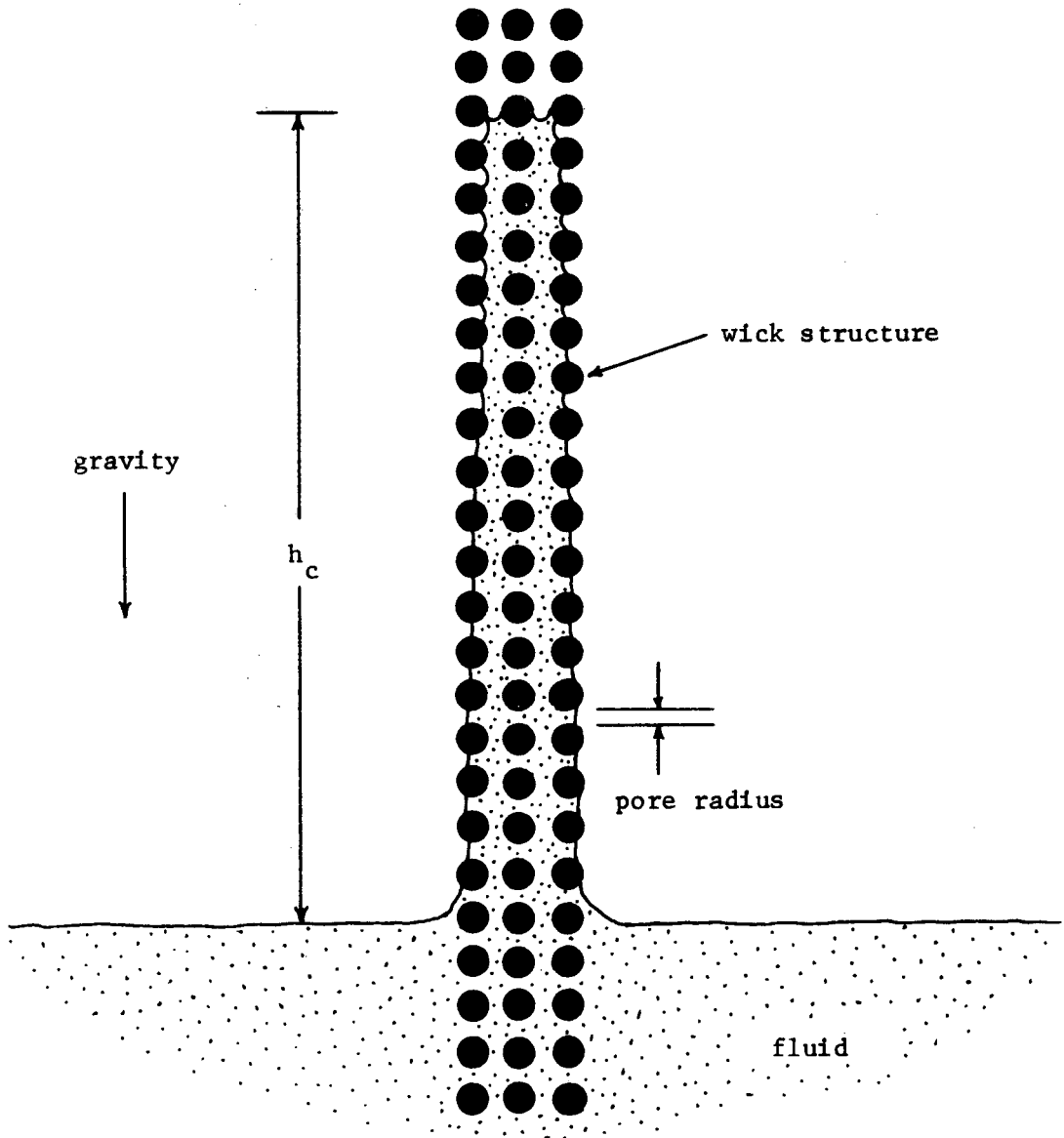


Figure 2. A Two-Dimensional Representation of a Capillary Wick, showing Vertical Hydrostatic Fluid Profile.

At this point, two important differences between the two schemes must be mentioned. First, the typical hydraulic radius of an EHD flow structure ( $s \approx .1$  to  $.5$  cm) is much larger than the pore size of a capillary ( $r_p \sim .010''$ ). Second, a remote voltage control is exerted over  $h$  which is not possible with  $h_{cap}$ .

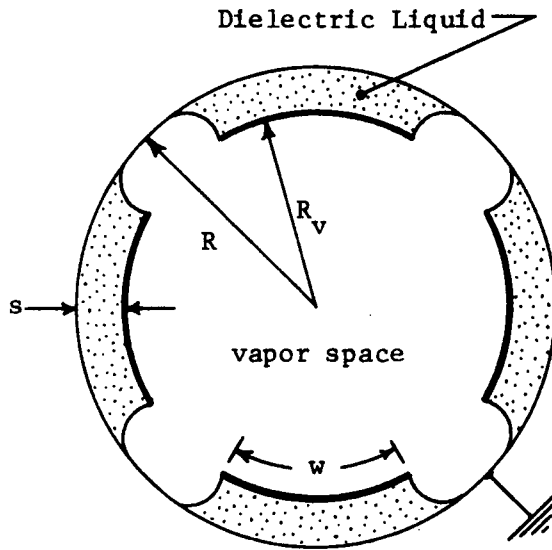
The most promising configuration of the electrohydrodynamic heat pipe is one which is very similar in form to artery heat pipes with threaded grooves.<sup>18</sup> The idea is merely to replace the capillary artery of a second-generation heat pipe with one or more EHD flow structures. See Figs. 3 and 4. The electrode structures guide and "pump" dielectric fluid from the condenser to the evaporator providing axial liquid flow. The circumferential threaded grooves provide for condensate flow into the EHD flow structures at the cooled end, and distribute this liquid to the surface at the heated end. One advantage seen immediately in this scheme is that EHD electrode structures provide much more intimate fluid contact between the arterial structures and the heat transfer surfaces, alleviating the need of feeder spokes. This may help to overcome problems related to the impeded transport of liquid into evaporator grooves.

#### B. Flow Dynamics

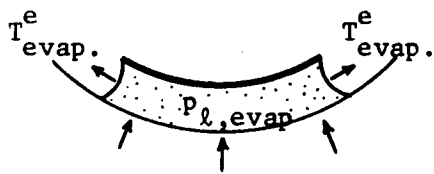
##### The Dielectric Pumping Head

Consider the very simple EHD heat pipe shown in Figure 3. It consists of a conducting metal tube with four thin strap electrodes running its length. These electrodes are insulated from and held at a high voltage with respect to the electrically grounded tube. The liquid in the heat pipe is maintained between the electrodes and the inner tube wall by the polarization force, with the vapor phase in the central core. This basic configuration serves as a prototype for all EHD heat pipes.

- n = number of EHD liquid flow structures
- R = radius of cylinder
- $R_v$  = radius of vapor space
- L = length of heat pipe
- w = width of electrode strap
- s = electrode spacing
- V = applied voltage

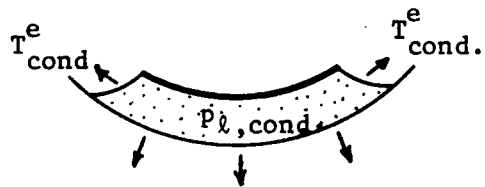


(a.) Cross-sectional View of simple EHD Heat Pipe.



(heat in)

(b.) Evaporator



(heat out)

(c.) Condenser

Figure 3. Prototype EHD Heat Pipe Using Parallel-Plate Flow Structures.

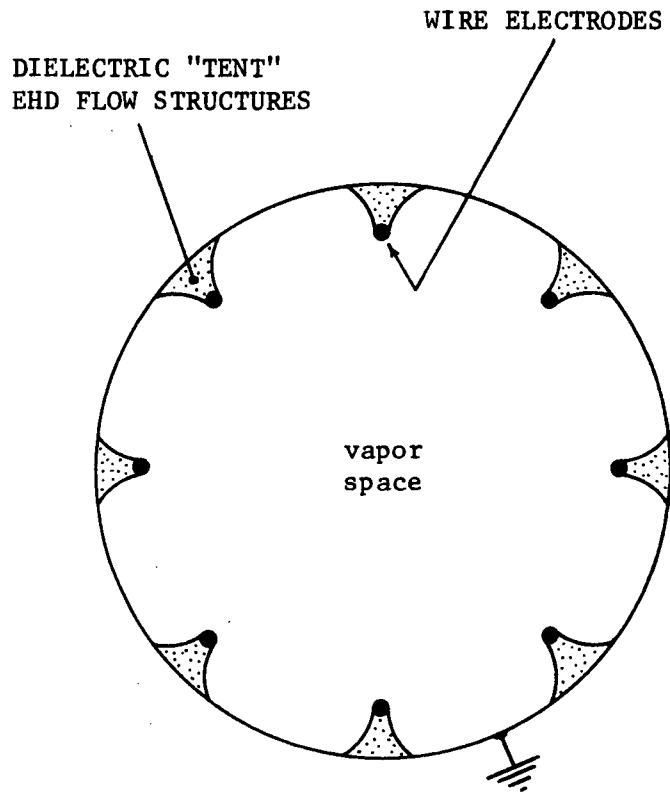


Figure 4. Possible EHD Heat Pipe Utilizing Dielectric "Tent" Flow Structures (Device Shown in Cross Section).

By writing the surface force balance equations at the evaporator and condenser ends, the dielectric pumping head may be determined.

$$P_{\ell, \text{evap.}} + T_{\text{evap.}}^e - P_{v, \text{evap.}} = 0, \quad (5)$$

$$P_{\ell, \text{cond.}} + T_{\text{cond.}}^e - P_{v, \text{cond.}} = 0 \quad (6)$$

where the subscripts correspond to liquid ( $\ell$ ), vapor ( $v$ ), evaporator (evap.), and condenser (cond.). Two more expressions for the pressures may be written in terms of the various pressure drops and the gravitational head:

$$P_{\ell, \text{cond.}} - P_{\ell, \text{evap.}} = \Delta p_{\ell, \text{viscous}} + \Delta p_{\ell, \text{shear}} + \rho_{\ell} g L \sin \phi \quad (7)$$

$$P_{v, \text{evap.}} - P_{v, \text{cond.}} \approx \Delta p_{v, \text{viscous}} + \Delta p_{v, \text{momentum}} \quad (8)$$

Equations (5-8) are combined to yield:

$$T_{\text{evap.}}^e - T_{\text{cond.}}^e - \rho_{\ell} g L \sin \phi = \Delta p_{\ell, \text{viscous}} + \Delta p_{v, \text{viscous}} \\ + \Delta p_{\ell, \text{shear}} + \Delta p_{v, \text{momentum}} \quad (9)$$

The dielectric pumping head,  $\Delta T^e$ , is defined using Equation (2).

$$\Delta T^e = \frac{(\epsilon_{\ell} - \epsilon_0) E_{\text{evap.}}^2}{2} - \frac{(\epsilon_{\ell} - \epsilon_0) E_{\text{cond.}}^2}{2} \quad (10)$$

$E_{\text{evap.}}$  and  $E_{\text{cond.}}$  are the transverse electric fields experienced respectively

by the liquid surfaces at the evaporator and condenser, and, for normal operation,

$$E_{\text{evap.}} > E_{\text{cond.}},$$

meaning that the liquid will bulge out further into the fringing field at the condenser than at the evaporator (this in continued analogy to capillary wick heat pipes). Refer again to Figure 3b and c.

Under proper conditions of fluid inventory, the maximum dielectric head is:

$$\Delta T_{\text{max}}^e = \frac{(\epsilon_l - \epsilon_o) E_o^2}{2}, \quad (11)$$

where  $E_o \approx V/s$  is the essentially uniform field between the electrode and the inner wall of the tube. The condition of maximum flow rate is obtained by using Eqs. (10, 11) in the flow expression Eq. (9). This is analogous to the case of liquid completely soaking the condenser wick of a capillary heat pipe, and receding well into the pores at the evaporator wick so that:

$$\left( \Delta p_{\text{cap}} \right)_{\text{max}} \approx \frac{2\gamma \cos \theta}{r_p} \quad (12)$$

where  $r_p$  is the wick pore size, and Eq. (12) represents the maximum capillary "pumping" head.<sup>19</sup>

#### Viscous Head Losses

In general for EHD devices both the vapor and liquid phase flows contribute to the viscous head loss. The liquid flows between what can be modeled as parallel plates, and the velocity distribution is described as essentially Poiseuille flow. The important difference between this flow situation and true two-dimensional Poiseuille flow is the presence of the

free surfaces, which are subject to the retarding shear force caused by the counter-flowing vapor. The vapor shear contribution to the liquid flow pressure drop is treated in the next sub-section, though only in an approximate way. The great difficulty of this fluid dynamics problem precludes any attempts at a general formal solution here.

For laminar flow,  $\Delta p_{\ell, \text{viscous}}$  is easily determined. A simple extension of the Blasius correlation<sup>20</sup> may be made to allow for the possibility of turbulent liquid flow. The result is

$$\Delta p_{\ell, \text{viscous}} = \frac{\dot{m}}{n} \cdot \frac{\mu_{\ell}}{\rho_{\ell}} \sim \frac{12 L_{\text{eff}}}{ws^3} \delta_{\ell} \quad (13)$$

where

$$\delta_{\ell} = \begin{cases} 1 & , \quad \text{Re}_{\ell} < 2200 \\ .00494 \text{Re}_{\ell}^{3/4} & , \quad \text{Re}_{\ell} > 2200 \end{cases} \quad (14)$$

and

$$\text{Re}_{\ell} = \frac{\dot{m}}{nw\mu_{\ell}} \quad (\text{the liquid Reynolds Number})$$

$$L_{\text{eff}} = \frac{2L_a + L_{\text{evap.}} + L_{\text{cond.}}}{2} \quad (\text{effective length}),$$

and  $\dot{m}$  is the total mass flow.

The vapor viscous pressure drop is

$$\Delta p_v = \frac{8L_{\text{eff}}\mu_v}{\pi\rho_v R_v^4} \cdot m\delta_v, \quad (15)$$

$$\delta_v = \begin{cases} 1 & , \quad Re_v < 2200 & ; \\ .00494 Re_v^{3/4} & , \quad Re_v > 2200 \end{cases} \quad (16)$$

and  $Re_v = \frac{2 \dot{m}}{\pi R_v \mu_v}$  , the vapor Reynolds Number.

### Momentum Effects on Vapor Flow

The total mass flow of vapor (and liquid) varies in the condenser and evaporator sections of a heat pipe, due respectively to the condensation mass removal and evaporative mass addition processes. The effect on vapor flow is analogous to that of mass injection and removal (suction). An additional net pressure drop term is introduced.<sup>21</sup>

$$\Delta p_{v, \text{momentum}} = \frac{\left(1 - \frac{4}{\pi^2}\right) \dot{m}^2}{8 \rho_v R_v^4} \quad (17)$$

Eq. (17) is commonly used in cylindrical heat pipes where the radial vapor flow is sufficiently large.<sup>21</sup> Such is expected to be the case in most EHD heat pipes of interest.

### Vapor Shear Forces

The flow of high-speed vapor in the opposite direction to liquid flow in a heat pipe can induce important shear forces at exposed liquid-vapor surfaces. This is more significant for axially grooved and EHD heat pipes due to the extensive unobstructed surface areas of the liquid flow structures. The shear traction is

$$\tau_v = \frac{f \dot{m}^2}{2 \pi^2 \rho_v R_v^4} \quad (18)$$

where  $f$ , the friction factor, is determined from graphic data.<sup>22</sup> For purposes of approximate analysis, useful limits on  $f$  may be placed,

$$.003 < f < .05 \quad , \quad (19)$$

with the higher limit of .05 being used as a conservative estimate. The pressure difference is then calculated as follows:

$$\Delta p_{\ell, \text{shear}} = \tau_v \cdot \frac{2L}{w} \quad (20)$$

### Summary

The use of Equations (13-20) with (8) and (10) produces a nonlinear equation in  $\dot{m}$ , the mass flow rate, in terms of the various system parameters and  $\Delta T^e$ . This equation may be solved numerically for  $\dot{m}$ , and thus the thermal throughput  $Q$  is determined.

$$Q = \lambda \dot{m} \quad , \quad (21)$$

where  $\lambda$  = latent heat of vaporization.

### C. Heat Transfer in EHD Heat Pipes

The previous section treats the flow dynamics without coupling it to the complex heat transfer process which actually drives the fluid. The logical next step is, then, to treat the heat transfer problems and to calculate the total temperature drop from the outside surface of the evaporator to the outside surface of the condenser. Several factors contribute to this overall temperature drop, including thermal conduction, vapor expansion, evaporation and condensation.

$$\Delta T_t = \Delta T_k + \Delta T_v + \Delta T_{\text{evap.}} + \Delta T_{\text{cond.}} \quad (22)$$

In this section follow quantitative discussions of these temperature drops. It is assumed in all analyses that the evaporation and condensation heat transfer processes are axially uniform.

Conduction Heat Transfer ( $\Delta T_k$ )

The transfer of heat from the outside to the inside tube surface at the evaporator (or vice versa at the condenser) is a simple conduction process. Since the tube walls are ordinarily quite thin, the linear approximation regarding heat flux is made.

$$Q/A \approx \frac{k \Delta T}{\Delta x} \quad (23)$$

where  $k$  is the thermal conductivity. Then the total conduction temperature drop (through the condenser and evaporator walls) may easily be calculated:

$$\Delta T_k = \frac{Q}{k} \left[ \frac{\Delta x_{\text{cond.}}}{A_{\text{cond.}}} + \frac{\Delta x_{\text{evap.}}}{A_{\text{evap.}}} \right] \quad (24)$$

where  $\Delta x$  is the condenser or evaporator wall thickness, and  $A$  is the condenser or evaporator surface area. Ordinarily, this conduction temperature drop is not appreciable for EHD or capillary heat pipes.

Vapor Expansion ( $\Delta T_v$ )

The vapor pressure drop due to viscosity and momentum effects gives rise to a slight expansion of the vapor as it moves from the evaporator to the condenser. A slight temperature drop attends this expansion. The Clapeyron-Clausius equation may be used to determine  $\Delta T_v$ .

$$\Delta T_v \approx \frac{T_b \Delta p_v}{\lambda \rho_v}, \quad (25)$$

where  $T_b$  is the boiling point of the working fluid. Typically,  $\Delta T_v$  is found to be less than 1°F, and is thus quite insignificant. It can only become large when the operating vapor pressure is very low, a condition not generally attractive for any heat pipe.

#### Evaporation Heat Transfer ( $\Delta T_{\text{evap.}}$ )

The effects of electric fields on evaporation and nucleate boiling heat transfer have been studied by a number of investigators,<sup>6-9</sup> and the EHD heat pipe proposed here offers the unique opportunity to utilize these effects as an integrated functional aspect of the device. This statement takes on importance when one considers the fact that the evaporation process imposes one of the upper limits on heat pipe operation and also generally accounts for a large portion of the total temperature drop. Any way in which the evaporation heat transfer process in a heat pipe can be enhanced is to be seriously considered.

The vaporization process in capillary wicks is not completely understood at this time, though it is generally agreed that the initiation of nucleate boiling ultimately limits the maximum heat flux in the evaporator, due to the detrimental effects of vapor bubbles upon liquid phase flow. For an EHD heat pipe, this limit is not expected to be critical for two reasons. First, the typical dimensions of EHD flow structures are too large to become clogged by such nucleated bubbles. Second, the presence of an electric field in a boiling liquid tends to suppress nucleation<sup>6</sup> and to alter the classically recognized boiling curve, so as to increase the peak nucleate boiling heat flux, by factors up to 2-3<sup>7, 9</sup>. Figure 5 shows a typical boiling curve with and without an applied electric field. Several physical mechanisms probably contribute to the enhancement of nucleate boiling; an

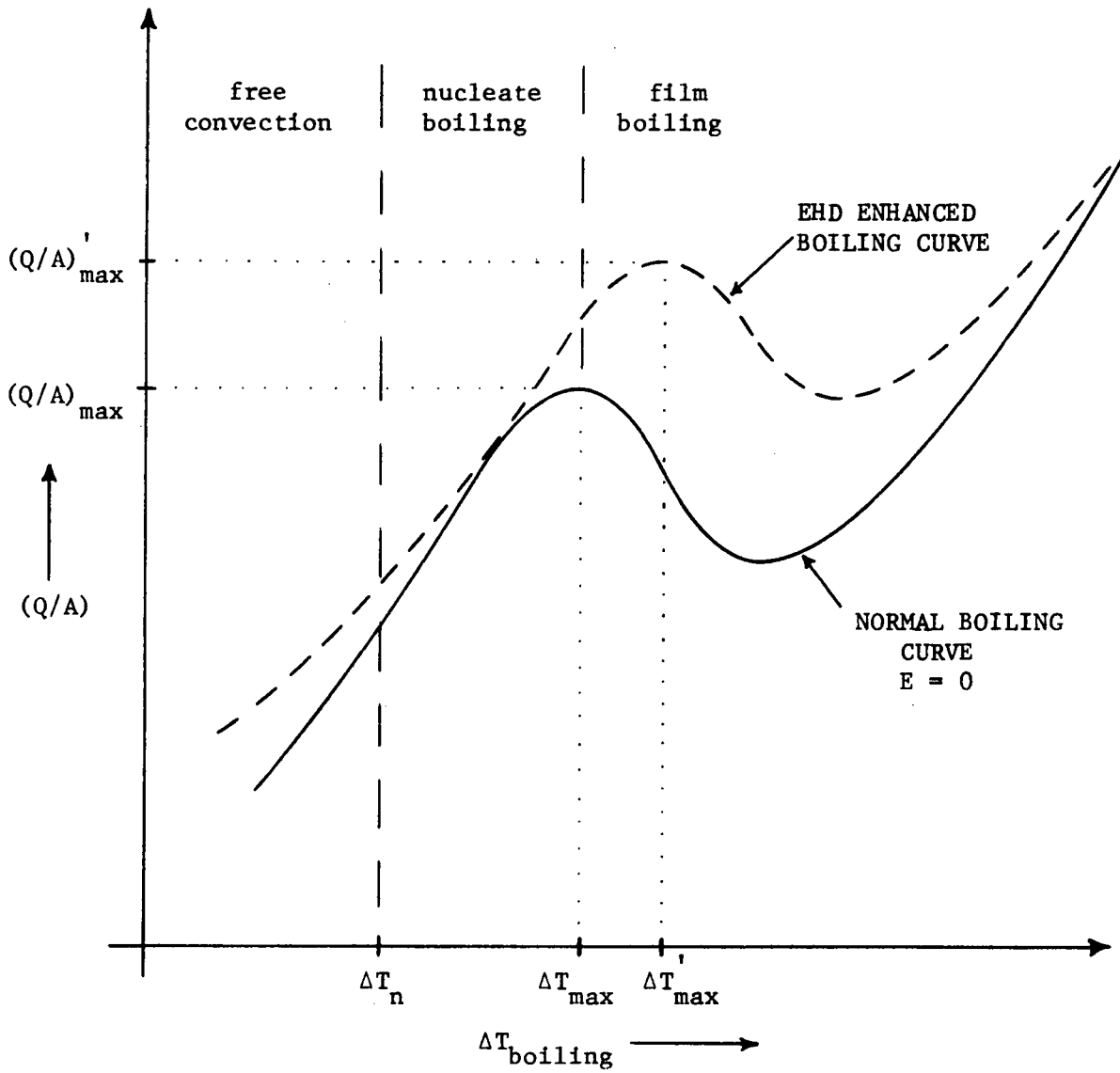


Figure 5. Typical Boiling Heat Transfer Curves with and without Gradient Electric Field Enhancement. Note that in general both  $(Q/A)_{\max}$  and  $\Delta T$  are increased by E field effects.

important one recognized by Choi<sup>6</sup> is the true dielectrophoretic force which tends to expel vapor bubbles from regions of higher electric field intensity. For the case of d-c electric fields, other electrophoretic forces which rely on free charge are doubtlessly important, too.<sup>9</sup>

Still, the conjecture that full nucleate boiling can be sustained does not necessarily mean that all EHD heat pipes will be advantageously operated in this regime. Reference to Figure 5 again indicates that, attendant with the increased maximum heat flux, will be an increase in the superheat  $\Delta T_{\text{evap}}$  needed to maintain this high thermal power level. In many heat pipes, this  $\sim 50^\circ\text{F}$  temperature drop will be considered excessive, especially in temperature control applications.<sup>23</sup> Thus, at first glance, the only real advantage of EHD boiling heat transfer is a significantly improved superheat tolerance and burn-out resistance.

The quantitative description of evaporation and boiling heat transfer is limited primarily to empirical correlations. An example is the peak nucleate boiling heat transfer flux:<sup>22</sup>

$$(Q/A)_{\text{max}} = .121 \cdot 10^{-5} \rho_v \lambda \bar{g}^{\frac{1}{2}} \left( \frac{\rho_l - \rho_v}{\rho_v} \right)^{0.6} \left( \frac{\text{watts}}{\text{sq cm}} \right), \quad (26)$$

where  $\bar{g} = g/g_0$ ,  $g_0 = 9.81 \frac{\text{m}}{\text{sec}^2}$ .

The temperature drop is also determined from an empirical correlation:<sup>24</sup>

$$\Delta T_{\text{max}} = 16.8 (Q/A)_{\text{max}}^{.293} \quad (27)$$

Though boiling is to be avoided in operation, Eq. (26) is useful in determining approximate values of attainable heat fluxes. (Remember that electric

field effects represent an additive factor to this correlation). The superheat expression Eq. (27) is of little or no value if the evaporator is threaded. The atmospheric boiling point values of  $(Q/A)_{\max}$  and  $\Delta T_{\max}$  are given in Table II for several candidate working fluids.

fluid	$(Q/A)_{\max}$ (watts/cm <sup>2</sup> )	$\Delta T_{\max}$ (°F)	@ $T_b$ (°F)
Freon-113	31.9	46	118
Freon-12	33.3	47	-21
Freon E-3	18.3	39	306
Dowtherm A	35.6	48	495
CP-9 (Monsanto)	31.0	46	567

Table II. Peak Nucleate Pool Boiling Heat Flux and approximate Superheat Values.

### Condensation Heat Transfer

Quantitative description of the condensation heat transfer process in an EHD heat pipe is not a simple task. The contributions of vapor shear forces, fluid convection, and polarization forces to the basic condensation phenomenon complicate the relatively simple Nusselt theory.<sup>22</sup> Still, some general remarks may be made.

There are two distinct types of condensation. In *film condensation*, the vapor condenses in a thin film which is swept away by gravity if the cooled plate is vertical and by other artificial means if the plate is horizontal. In *dropwise condensation*, the vapor condenses, but then the

condensate on the plate gathers into drops which grow until they roll off or are otherwise removed. The latter process can be promoted if the cooled plate is specially treated so as not to be wetted by the condensed liquid. Dropwise condensation is a much more efficient heat transfer process, because of the relatively large surface areas which remain exposed. (It is also hard to maintain for extended periods). Film condensate, on the other hand, provides its own insulating layer which, once formed, impedes further heat transfer.

Polarization EHD effects may be utilized to promote a pseudo-dropwise condensation process, where the electrode structures collect the condensate away from the surface as fast as it appears (see Figures 3 and 4). The electrode structures' function is then similar to that of droplets, but with the polarization force taking the place of surface tension. With its more generally distributed electric field gradient, the "dielectric tent" configuration of Figure 4 appears more suited to condensation in an EHD heat pipe than the parallel-plate design of Figure 3.

Nominal limits on heat transfer coefficients for film and dropwise condensation of water are as follows:<sup>22</sup>

$$h_{\text{film}} = .25 \text{ to } .63 \frac{\text{watts}}{\text{cm}^2\text{-}^\circ\text{F}}, \text{ (film);} \quad (28)$$

$$h_{\text{dropwise}} = 3.15 \text{ to } 25 \frac{\text{watts}}{\text{cm}^2\text{-}^\circ\text{F}}, \text{ (dropwise).} \quad (29)$$

These values are for water which has a latent heat 5 to 10 times that of most organic dielectric fluids. Thus, the attainable coefficients for EHD heat pipe evaporators are expected to be lower.

### Threaded Groove Heat Transfer

Threading the inner wall of a cylindrical heat pipe, at both the evaporator and condenser ends, permits the attainment of very high heat transfer rates with very small temperature drops.<sup>18, 25</sup> Capillary heat pipes coupling threaded grooves with arterial wicks for axial flow have attained effective thermal transport factors in the range of 50,000 watt-inches, using ammonia as the working fluid.<sup>26</sup> It is suggested that the liquid flow structures of EHD heat pipes (see Figs. 3 and 4) are entirely compatible with threaded grooves. In the proposed device, the EHD electrode structures would provide axial flow and the grooves would provide circumferential flow. Such a hybrid heat pipe would thus employ the distinct advantages of both capillarity and polarization EHD.

Evaporation and condensation heat transfer at grooved surfaces is not well understood. Still, a qualitative picture, generally agreed upon, exists. First, the evaporation process occurs in regions of very thin liquid film at the lands between adjacent grooves.<sup>16</sup> This results in high heat transfer rates with low driving thermal potentials. Heat transfer coefficients from  $\sim 0.3$  to  $\sim 0.8 \frac{\text{watts}}{\text{cm}^2 \cdot ^\circ\text{F}}$  ( $1000$  to  $2500 \frac{\text{Btu}}{\text{hr-ft}^2 \cdot ^\circ\text{F}}$ )<sup>18, 26</sup> have been experimentally obtained (with ammonia, @  $\Delta T_{\text{evap}} \sim 10^\circ\text{F}$ ), and at least some data from TRW indicates that these coefficients are *increasing* functions of  $\Delta T_{\text{evap}}$ .<sup>18</sup> Moritz has attained an evaporation heat flux of  $145 \text{ watts/cm}^2$  for water.<sup>27</sup>

Condensation is likewise enhanced. The condensate collects in the grooves, promoting a pseudo-dropwise condensation process which is superior to laminar film condensation, due to the constant exposure of the sub-cooled lands to vapor. Surface tension effects presumably draw the liquid into the grooves. The measured heat transfer coefficients are typically  $\sim 20\%$  *higher* than the evaporator values.<sup>18</sup>

It is not understood whether or not the presently realized performance of threaded groove evaporators and condensers can be significantly improved upon. One paper on this subject, by Bressler and Wyatt,<sup>28</sup> points out that optimization based upon groove dimensions and (possibly) configuration is a valuable exercise. From their theoretical calculations and limited (isolated groove) data, they predict heat transfer coefficients of  $\sim 30$  watts/cm<sup>2</sup>-°F for water; from their curves,  $\sim 3$  watts/cm<sup>2</sup>-°F can be predicted for Freon-22. Reference to the available data, as reviewed above, indicates that such coefficients have not yet been observed in threaded-groove heat pipes. Whether or not this is due to the non-optimized nature of the grooves in working heat pipes is an open question.

The proposal to use threaded grooves for circumferential flow in an EHD heat pipe is important, principally because EHD devices are limited to the relatively low performance organic dielectric fluids. Thus, every means available must be utilized to improve evaporation and condensation heat transfer rates. The compatibility of EHD structures to grooves appears good. Liquid contact with the grooves does not rely upon the crucial contact of the wall with feeder wicking structures; the electric "walls" of the flow structure serve this function very well. Thus, any problem normally associated with getting liquid out of the axial flow structures into the grooves\* should be alleviated. The presence of the electric field in the vicinity of the grooves should also help prevent nucleation.

At the condenser, the EHD flow structures should act to assist heat transfer by active collection of condensate away from the grooves. Though the magnitude of this effect cannot be assessed at this stage of the research

---

\* Moritz<sup>27</sup> recognizes this as a significant problem in threaded artery heat pipes.

program, it is clear that it can only act to *enhance* heat transfer.

In Appendix A, the predicted performance of two EHD heat pipes is considered in light of the limited information presently available about the attainable heat transfer coefficients in evaporators and condensers. The calculations show that with close attention paid to groove optimization, the design and construction of rather high-performance EHD heat pipes will be possible.

#### D. Entrainment

If the difference in velocity between the liquid and vapor flows becomes substantial, a Kelvin-Helmholtz type of instability occurs, the liquid surface can become ruffled, possibly resulting in the entrainment of liquid droplets into the vapor stream. It may be anticipated that this entrainment will be a greater problem in EHD flow structures than in capillary wicks, because the free surface areas are typically much larger in EHD structures. Actually, here the electric field replaces the influence of capillary forces to balance the destabilizing mechanism, and an electrical Weber number may be defined to predict the onset of this instability.

$$We^E \approx \frac{\rho_v V_v^2}{(\epsilon_l - \epsilon_o) E_o^2} \quad (30)$$

If this parameter becomes greater than one, the destabilizing tendency of the high velocity vapor flow dominates the stabilizing electrical force, thus introducing the possibility of instability and entrainment. Such an occurrence may be much more disruptive with EHD heat pipes, because of the open nature of their liquid flow paths. The shielding of the liquid flow from high velocity vapor shears may become a consideration in EHD heat pipe design.

E. EHD Wavespeed Limit

A new limit on heat pipe operation, based on a property solely encountered in EHD flow structures, may be predicted here. The peculiar class of flows which the structures of Figures 3 and 4 represent, exhibits the feature of nonlinear surface wave phenomena analogous to the gravity waves known from open channel flow.<sup>14</sup> A condition of criticality is reached when the velocity of the liquid approaches the surface wave celerity. With the structure in a horizontal configuration (without the gravitational body force to accelerate the liquid), an attempt to vary end conditions so as to produce super-critical flow results in a nonlinear hydraulic jump which occurs somewhere along the length of the structure. Jones has observed these shock waves, and has noted that they can be disruptive enough to present a limit on EHD heat pipe operation.<sup>14</sup> The condition of flow criticality is thus taken as an operational constraint on EHD heat pipes. The condition is:

$$v_{\ell} < v_{\text{EHD}} \quad , \quad (31)$$

where  $v_{\text{EHD}}$  is the EHD surface wave celerity, and must be calculated or measured as a function of voltage.<sup>3, 14</sup>

It is of interest to conjecture on the possibility of the existence of a similar limit on arterial heat pipes. Certain types of arteries should be capable of supporting surface waves analogous to the EHD surface waves already mentioned, and a consideration of the flow dynamics might lead to the prediction of nonlinear capillary hydraulic jumps.

#### IV. RUDIMENTS OF THE DESIGN OF EHD HEAT PIPES

EHD heat pipes must be designed and constructed with a rather large number of constraints in mind. This section outlines the topics of fluid selection and design optimization, and then lists the presently recognized operational limits.

##### A. Fluid Data

###### Classification

To characterize the suitability of a candidate working dielectric fluid for use in an EHD heat pipe, almost all of the fluid data used for capillary devices is required, plus a certain amount of electrical data. The Table III below classifies and lists the needed data.

---

<u>Physical/Transport</u>	<u>Thermodynamic</u>	<u>Electrical</u>
liquid, vapor density	vapor pressure	liquid dielectric constant
molecular weight	latent heat of vaporization	liquid electric conductivity
liquid, vapor viscosity	liquid, vapor specific heats	liquid, vapor breakdown strength
surface tension	specific heat ratio	
boiling and freezing points		
liquid thermal conductivity		

Table III. Useful Working Dielectric Fluid Properties-Classification

---

Further, it is necessary to know these properties over the temperature range which corresponds to the operating range of a specific heat pipe application.

This is no mean task, considering the limited availability and existence of certain data for dielectric fluids.

### EHD Fluid Transport Factor

A grouping of fluid properties has been identified, which provides a measure of the relative merits of various dielectric fluids for EHD heat pipes. This "figure of merit" is analogous to the liquid transport factor used to compare heat transfer fluids for capillary devices. The physical significance of the two factors is slightly different, however, and with dissimilar units, they cannot be meaningfully cross-compared. The EHD liquid transport factor is

$$N_{\text{EHD}} = \frac{(\epsilon_{\ell} - \epsilon_0) E_b^2 \lambda \rho_{\ell}}{\mu_{\ell}} \quad (32)$$

where  $E_b$  is the breakdown field strength of the saturated vapors of the dielectric fluid. This value is used rather than the normally higher liquid breakdown strength to provide a safety factor in operational situations when the liquid might be temporarily displaced from high electric field intensity regions by sudden shocks or strong vibration. The transport factor for a few fluids is plotted versus temperature in Figure 6. The curves for Freon-113<sup>®</sup> and Freon-12<sup>®</sup> (Dupont) do not indicate it, but it is expected that  $N_{\text{EHD}}$  peaks at some temperature for both these fluids and then decreases, due to the fact that the breakdown strength exhibits no further increase after some critical vapor pressure value is reached.

### The Wicking Height

A liquid dielectric will rise between vertical electrode plates, when stressed by high voltage, as Figure 1 demonstrates. The height to which it will rise is a function of the maximum electric field the vapors will tolerate

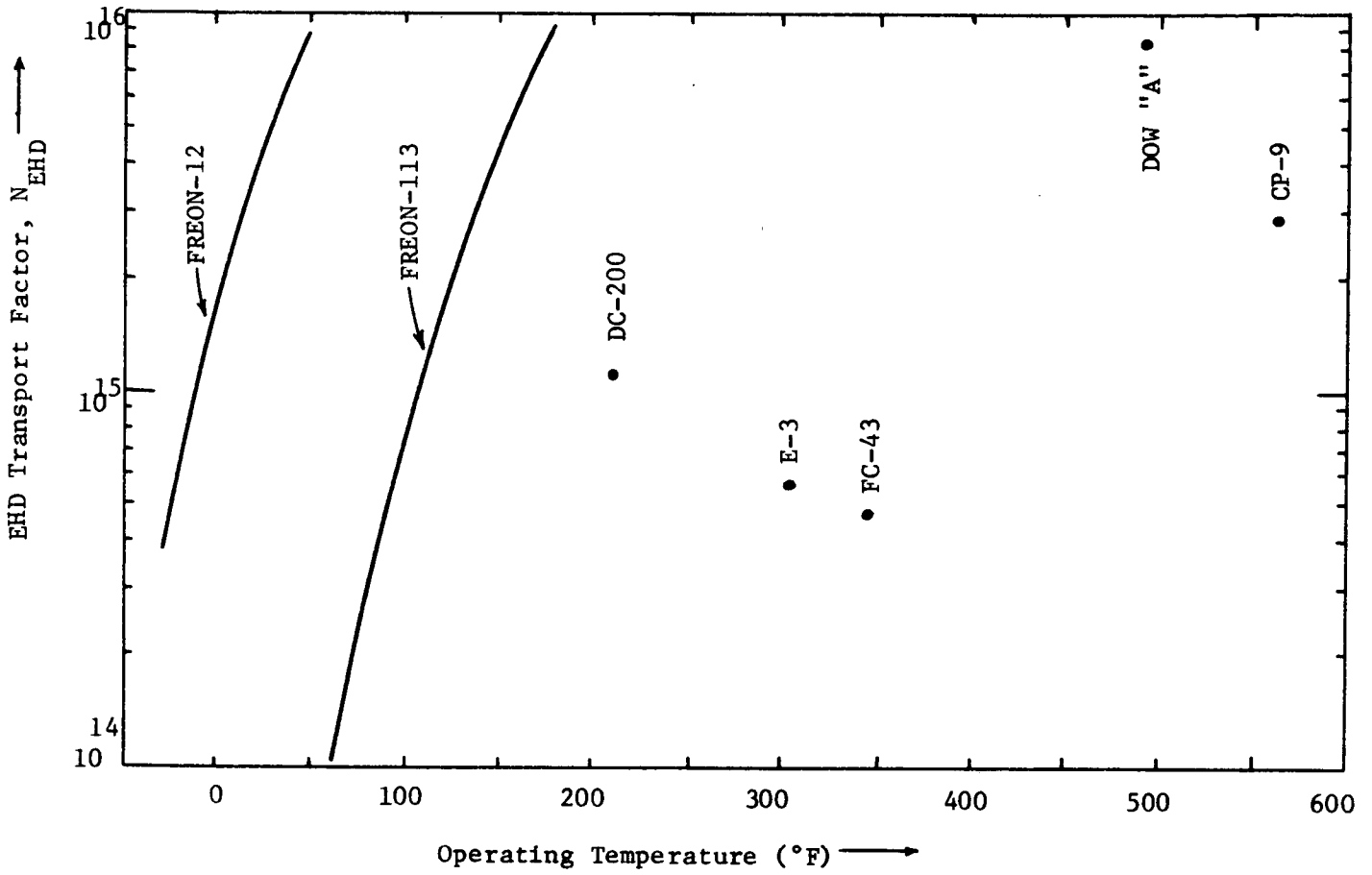


Figure 6. EHD Transport Factor for Various Dielectric Liquids.

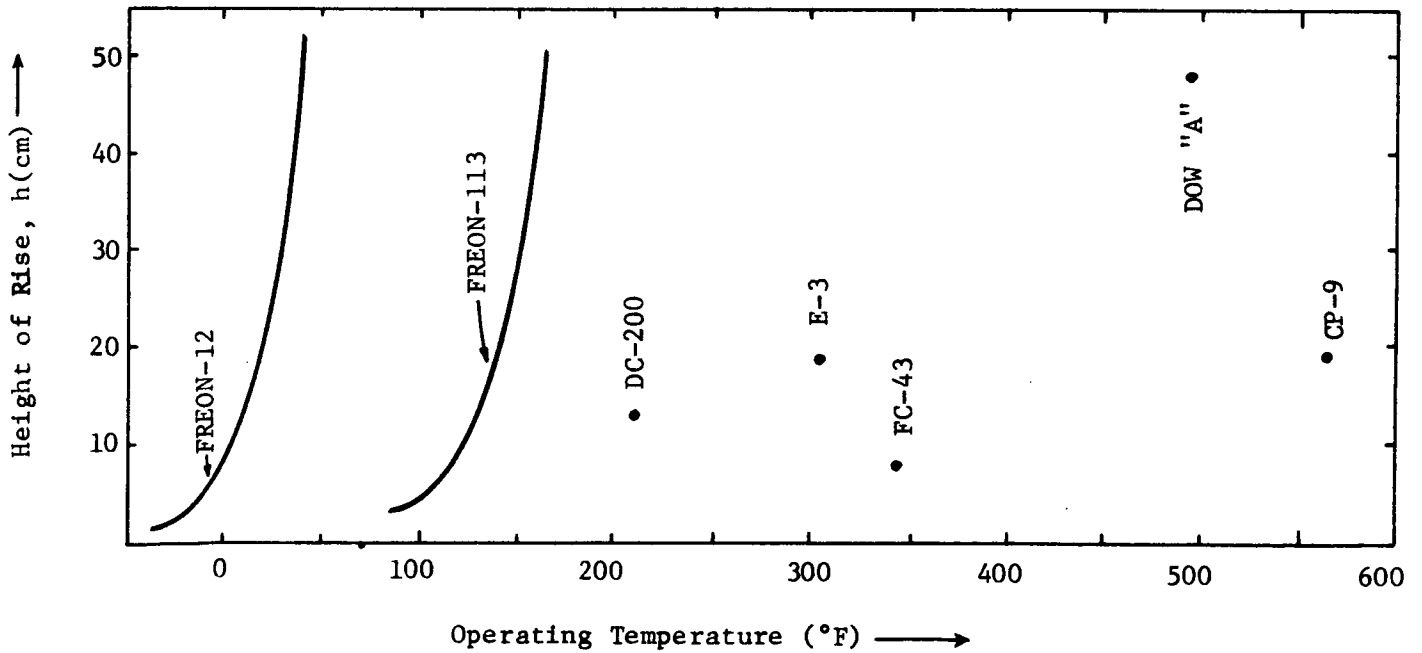


Figure 7. Available Height of Rise for Various Dielectric Liquids.

before electrical breakdown ( $E_b$ ). Figure 7 contains plots of this height as a function of temperature. These plots indicate the very strong dependence of  $E_b$  on the vapor pressure  $p_v(T)$ . The importance of this height is obvious in that it is a measure of how effectively an EHD heat pipe will perform under adverse gravity (acceleration) conditions.

### Summary

The decision regarding fluid choice is most limited by the operating temperature range specified for the application, and probably an intelligent decision may be made by reference to Figures 6 and 7. The various fluorocarbon, silicone, and organic dielectric fluids represented there provide fairly complete coverage over the  $-100^\circ\text{F}$  to  $+500^\circ\text{F}$  temperature span. The fluids Freon E-3<sup>®</sup> (Dupont), Dowtherm A<sup>®</sup> (Dow), and CP-9 (Monsanto) appear to be the best all-around candidates for working fluids, and their temperature ranges conveniently fall between those of water and liquid metal heat pipes, thus suggesting their special value in EHD heat pipe technology. The Table IV provides fairly complete data on the atmospheric boiling point properties of the liquid and vapor phase of these and a few other fluids.

### B. EHD Heat Pipe Optimization

The optimization of EHD heat pipe performance is a more meaningful procedure than that of capillary devices, because no uncertainties about the statistical distribution of wick pore sizes exists; that is, electrode spacings are completely controlled by the designer. Also, and within limits, the designer has a direct control on the operating voltage. There is no analogous design flexibility with capillary structures, because: (i) surface tension is not variable for a given fluid; and (ii), the average pore size and size distribution are fixed for a given wick material. Thus, at least

FLUID	PHYSICAL / TRANSPORT								THERMODYNAMIC				ELECTRICAL			
	$\rho_l$ Liquid Density (gm/cm <sup>3</sup> )	$\rho_v$ Saturat- ed Vapor Density (gm/liter)	MW Molecular Weight (AMU)	$\mu_l$ Liquid Viscos- ity (poise)	$\mu_v$ Vapor Viscosity (poise)	$T_b, T_f$ Boiling and Freezing Points (°F)	$k_l$ Liquid Thermal Conduc- ivity  Watts m-°C	$\sigma$ Surface Tension  dynes cm	$\lambda$ Latent Heat of Vaporiza- tion  joules gm	$c_l$ Liquid Specific Heat  cal gm-°C	$c_p$ Vapor Specific Heat  cal gm-°C	$\gamma$ Vapor Specific Heat Ratio	$(\epsilon_l/\epsilon_0)$ Liquid Dielec- tric Conduc- tivity	$\sigma_l$ Liquid Electric Conduc- tivity  mhos m	Liquid Breakdown Strength (KV/cm)	$E_b$ Vapor Breakdown Strength (KV/cm)
Dupont Freon- 113	1.51	7.38	187.39	.0051	.00011	$T_b=117.6^\circ\text{F}$ $T_f=-31^\circ\text{F}$	.066	15.9	147.	.218	.161	1.08	2.33	$<10^{-12}$	173.	156.
Dupont Freon-12	1.485	6.33	120.92	.00396	.000107	$-21.6^\circ\text{F}$ $-252^\circ\text{F}$	.071	16.5	165.	.232	.145	1.137	2.36	-	-	93.
Dupont Freon E-3	1.41	18.4	618.12	<.004	-	$306^\circ\text{F}$ $-160^\circ\text{F}$	.0653	14.2	60.8	.24	-	-	2.58	$<2.5 \cdot 10^{-13}$	224.	194.
Dow Dowtherm A	.852	3.957	-	.0027	.000103	$494.8^\circ\text{F}$ $53.6^\circ\text{F}$	.1125	35.7	297.	-	.435	1.03	3.26	$2.56 \cdot 10^{10}$	208.	>200.
Monsanto CP-9	.776	4.34	196.3	.00241	.000169	$562-573^\circ\text{F}$ $-70^\circ\text{F}$ (pour point)	.1195	38.1	264.	.637	.445	-	2.50	$<10^{-12}$	158.	-
3M FC-43	1.54	-	-	.00262	-	$345^\circ\text{F}$ $-58^\circ\text{F}$	.0675	16.0	70.	.27	-	-	1.71	$<4 \cdot 10^{-13}$	220.	>138.

a... @ 25°C, 1 atmos.

b... @ 60°C, 1 atmos.

c... @140°F

d... @ 104°F

e... estimated

f... @300°F

g... @ 22°C

h... @500°F

i... @100°C

Table IV. Properties of Selected Dielectric Heat Transfer Fluids.  
(Unless otherwise indicated, all properties are measured  
at atmospheric boiling point, and saturation condition  
if applicable.)

one part of the criticism made by Marcus<sup>16</sup> with regard to standard heat pipe optimization procedure is not relevant to the analogous methods employed with EHD heat pipes.

On the other hand, the present limited understanding of evaporation and condensation in EHD heat pipes forces us to use an optimization criterion which Marcus rightfully questions.<sup>16</sup> This is an optimization based upon purely hydrodynamic considerations, i.e., a minimization of the total vapor/liquid flow resistance. While such a procedure is of only limited value in the general problem of heat pipe design, it still produces theoretical results which indicate the scope of possibilities for EHD devices. Thus, the details of the method are reviewed in this report. Carrying through with this analysis ultimately allows an improved picture of the various performance trade-offs to emerge.

#### The Optimization Procedure

The EHD heat pipe with "parallel-plate" EHD flow structures, shown in Figure 3, was chosen because a fairly complete model for the dynamics has already been successfully used elsewhere.<sup>2, 3</sup> The procedure is merely to vary electrode spacing  $s$  and applied voltage  $V$  so as to maximize flow rate for a pipe of given diameter and length. The same optimization has been done for several working fluids, all operating at their atmospheric boiling points. (In design practice, the optimization process would take fluid selection into account.)

Given the heat pipe diameter, length, operating pressure (or temperature), and the working fluid, the heat flux (throughput) is a single-valued function of electrode spacing  $s$  and voltage  $V$ .

$$Q(s,V) = \lambda m(s,V) \quad (33)$$

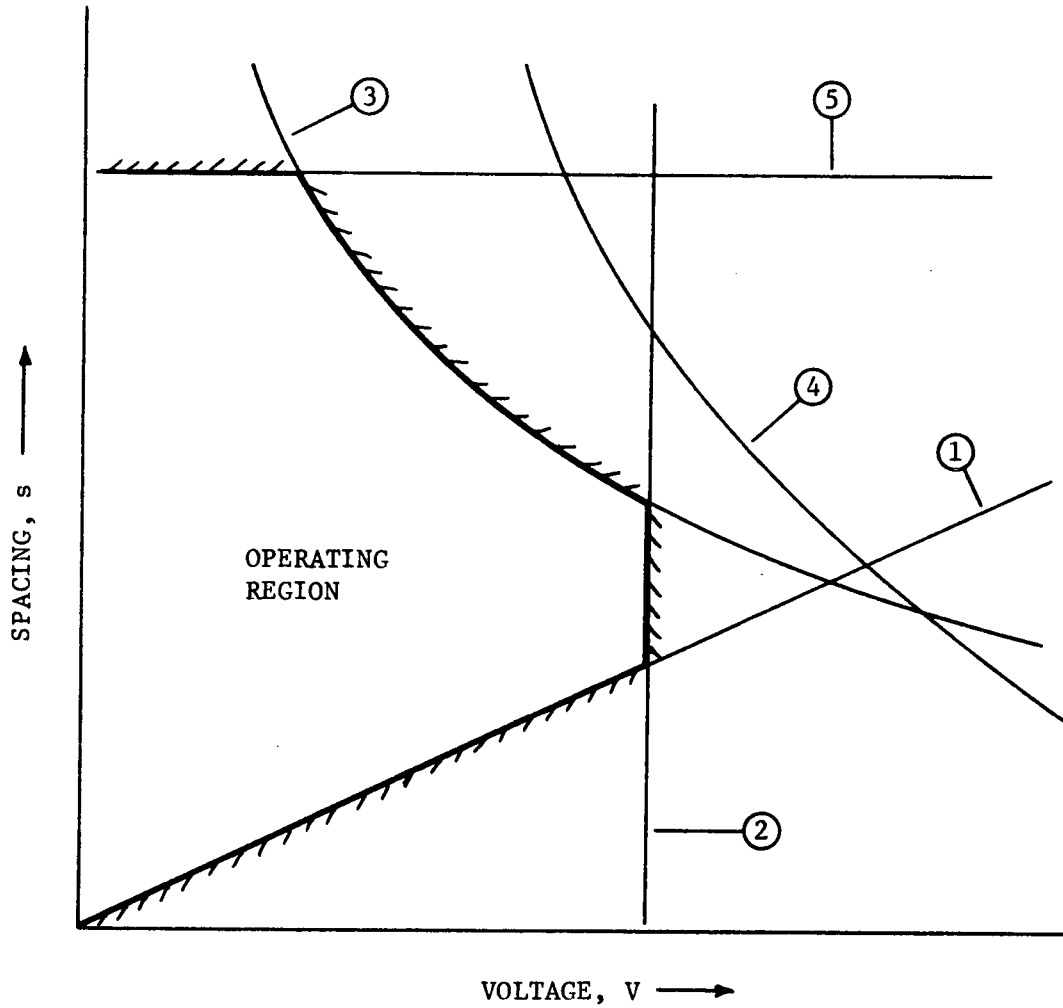
The optimization is thus performed in  $(s,V)$  space. The maximization is not a simple process of taking partial derivatives and eliminating saddle points, however. Numerous constraints must be placed on the allowable values of  $s$  and  $V$ . Figure 8 shows the usable operating region in  $(s,V)$ .

It is easily shown that  $m(s,V)$  increases monotonically with  $V$  for constant  $s$ . Thus, we look for the maximum value of  $m$  along the right-hand edge of the operating region, as defined by various portions of the curves ① through ⑤. Any values chosen outside the operating region as defined in Figure 8 will result in an encounter with some physical limitation detrimental to performance.

#### System Constraints

Operating limits serve as constraints upon optimization; they are enumerated and briefly discussed here.

- (1) Vapor Breakdown Limit. Considerable caution must be exercised to avoid electrical corona and breakdown phenomena. For lack of better data, it is assumed that the breakdown of vapor is proportional to  $s$  at constant vapor density. (This assumption is accurate for typical operating pressures if the electric field is essentially uniform with no strong gradients, normally avoidable when sharp points and corners are eliminated.) Thus, the curve ① is linear in  $(s,V)$  space. Quite often an optimized heat pipe operates very close to the breakdown limit. The possibly catastrophic nature of electrical breakdown in the closed environment of an EHD heat pipe suggests the advisability of including a safety margin in the



- ① Vapor Breakdown Limit
- ② Voltage Supply Limit
- ③ EHD Wavespeed Limit
- ④ Vapor Sonic Limit
- ⑤ Size Limit

Figure 8. Theoretical Operational Limits of EHD Heat Pipe in (s, V) Space.

ultimate design of high-reliability devices. Further, the detrimental nature of corona on vapors such as fluorocarbons for extended periods may require consideration. Fortunately, the natural tendency of liquid dielectrics to collect in regions of high electric field intensity, thus providing excellent insulation where it is most needed, is an ameliorating factor.

- (ii) EHD Wave Celerity Limit. As mentioned in section III.E, the liquid flow velocity is constrained by the finite EHD surface wave velocity of the flow structure. By changing Eq. (28) into an equality, a relation between  $s$  and  $V$  is obtained, which is represented by the curve ③ in Figure 8. Generally, this limit is less often encountered in EHD heat optimization than the breakdown limit, (i).
- (iii) Vapor Sonic Limit. This limit, usually of importance for capillary heat pipes operated at low vapor pressures (especially during cold startup), is not generally important, compared to breakdown and the EHD wave speed. It is approximately represented by the curve ④ in Figure 8.
- (iv) Voltage Supply Limit. For practical design consideration, it is appropriate to take into account the possibility of limited high voltage availability. This is particularly true if the intended application is in spacecraft systems. Though an EHD heat pipe requires very little electrical power (typically, less than one watt), still relatively high voltage is necessitated (from 20 to 50 kilovolts).

This presents little problem on the ground, but in space craft it can be quite a severe constraint. The curve ② in Figure 8 illustrates the form which this constraint takes in (s,V) space.

- (v) Size Limits. For the designs of Figures 3 and 4, a limit exists on how closely adjacent EHD liquid flow structures may be placed before their fringing fields commence to interact. Note that if  $w$ , the electrode width in Figure 3b, is kept constant, the structures must eventually start to interact as  $s$  is increased. Thus, the curve ⑤ represents this limit in (s,V) space.

Other operational limits certainly exist. One, the entrainment limit, shows itself to be important. However, there appear to be suitable ways of minimizing its effects, and thus it has been suppressed in the optimization outlined in Figure 8. The boiling and condensation processes provide further constraints on optimization, which are based on the maximum  $\Delta T_t$  to be tolerated in operation. This kind of limit imposes no constraints on (s,V), but instead can put an upper bound on total heat throughput which is lower than the hydrodynamic limit. The ultimate effect is to make the entire optimizing procedure a questionable method.

Typical results of the hydrodynamic optimization of an EHD heat pipe are given in the Appendix A. The various performance measures are calculated, and, to avoid the mistake of completely neglecting evaporator and condenser heat transfer, consideration is given to the compatibility of these processes to the optimized design. By this method, we can easily pick out any device which requires an obviously unattainable evaporation or condensation heat transfer coefficient.

## V. SUMMARY

The purpose of this last section is to assemble an overall picture of the electrohydrodynamic heat pipe, its presently recognized limitations, and its advantages relative to capillary devices. It must be kept in mind that the application of electric field phenomena to heat pipes can take a number of forms besides the use of EHD flow structures for wicking, as shown in Figures 3 and 4. A short section on optional features is included here, in order to indicate the extensive possibilities of applying electric field effects to heat pipe technology.

The initial thrust of this research was to consider the feasibility of EHD heat pipes which would successfully compete with state-of-the-art capillary devices. Thus, the tendency is to compare them to the high performance artery-threaded groove models which use water (or ammonia). This is not strictly appropriate, due to differing usable temperature ranges of water (or ammonia), and the organic fluids typical of EHD devices. Neither does such a comparison take into account some of the special features of EHD heat pipes, such as on/off control and 100% reliable priming. Still, the similarities of artery-threaded groove and EHD flow structure-threaded groove designs are so striking as to invite comparison. This subject will be covered in a future research report.

### The Wicking Limit (in organic heat pipes)

The tendency is to avoid, if possible, the design and use of organic fluid heat pipes, due to the relatively poor characteristics of these fluids. The same is essentially true of cryogenic fluids. Thus, any method whereby organic (or cryogenic) fluid heat pipe performance can be improved upon is of some interest. Basiulis and Filler state that most

organic fluid heat pipes are wick-limited.<sup>15</sup> If this is true, then the EHD heat pipe can be thought of as a boon, because, for practical purposes, the use of EHD flow structures effectively eliminates the wick limit. It does this not by increasing the effective pumping head, but by *drastically* decreasing the liquid pipe friction. In almost any situation where the use of organic fluids is required, due to the specified temperature range, then consideration of the EHD heat pipe is warranted. As with any organic fluid model, the electrohydrodynamic heat pipe enjoys the advantages of insensitivity to magnetic field effects, good materials compatibility, and relatively low working fluid costs.

#### Priming and Startup

The high performance artery heat pipe exhibits an unfortunate tendency toward unreliable priming,<sup>16</sup> and while this problem is receiving much attention now, it is not yet solved. The EHD heat pipe has no such drawback; priming is obtained *with 100% reliability*, merely by applying the operating voltage. This is because the EHD flow structure does not rely on uncertain wick-fluid wetting conditions, which can be drastically affected by minute impurities. To prevent arcing, it may sometimes be advisable to bring up the voltage to its operational level over a period of a few seconds in order to allow the liquid adequate response time and to minimize sloshing, but the procedure is purely precautionary and will not affect priming. This feature may be of considerable importance in solving the startup dynamics problems of some heat pipes.

#### Susceptibility to Boiling

Boiling in the wick of conventional heat pipes, or the mere presence of bubbles in the artery of high performance models, is detrimental to performance. Studies of EHD enhanced boiling heat transfer indicate that electric

field effects suppress nucleation, and, thereby, increase the superheat tolerance.<sup>6</sup> Also, in the event of bubble formation, electric field gradients can be used to force the bubbles out of the liquid into the vapor space. Thus, properly designed EHD flow structures have the ability to free themselves automatically of bubbles (which would tend to clog a capillary artery).

### Condensation

Though the discussion in this report concerning condensation (in section III.C) is the least quantitative of the sections on heat transfer, a qualitative point may be made. It has been adequately illustrated that gradient-featuring electric fields assist in the collection of condensate in a pseudo-dropwise process.<sup>10</sup> This indicates at least some enhancement of the heat transfer process in the condenser of EHD heat pipes. This point is important, because, as Appendix A indicates, condensation (with evaporation) heat transfer is apt to impose an important limit on operation.

### Heat Pipe Control

The ability to control externally the thermal throughput of a heat pipe is extremely desirable for several applications, such as temperature control, etc. Such control generally falls into two categories: continuous (applied to temperature control applications); and on/off control. Marcus describes three basic classes of mechanisms employed in heat pipes to achieve such control: liquid flow control, vapor flow control, and condenser flooding (via non-condensable gas or excess fluid)<sup>29</sup>. Of these three methods, condenser flooding is the most promising, and, in particular, a number of non-condensable gas "plug" controlled heat pipes have been tested successfully. A small amount of work has been performed on vapor flow controlled heat pipes,

but almost no effort has been directed toward liquid flow control. The lack of effort in developing the latter system is understandable when one considers the difficult nature of controlling the wicking properties in a heat pipe without elaborate servomechanisms. Further, Marcus suggests the possible difficulty in turning off such a device rapidly, due to fluid inertia.<sup>29</sup>

The EHD heat pipe enters the heat pipe control picture with a capability of direct voltage control of the pumping process, analogous to varying the surface tension in a capillary device. It should be classed as a liquid flow control technique, but not of any type previously envisioned. The liquid flow path is not obstructed by changing the voltage, rather the pumping head itself is controlled. For constant temperature evaporators, this approach leads to thermal control, continuous from *very* close to zero to maximum throughput. Because the control linkage is purely electrical, mechanical apparatus is obviated. It is not possible to conjecture at this point as to the on/off step response time of EHD heat pipes. In any case, EHD heat pipes show considerable initial promise in applications of thermal switching.

By proper design of auxiliary electrode structures in EHD heat pipe condensers, some pseudo-condenser flooding control might be achieved, but this idea is still in its formative stages.

#### Some Optional Design Features

- (i) In either capillary arteries or in certain types of EHD flow structures, it is possible to incorporate ion-drag pumping into the flow circuit, with the ultimate effect of enhancing the liquid flow.
- (ii) An EHD effect might be utilized to promote the priming of arterial wicks. Such a concept might be employed merely to assist the priming process when needed, or it could be incorporated into a hybrid EHD-capillary artery, with

capillarity providing the motive pumping force, and EHD effects insuring reliable priming and keeping the artery free of bubbles.

(iii) The evaporation or condensation process in a conventional heat pipe might be controlled by electric field effects, the result being a voltage-controlled capillary device.

### Conclusion

To summarize, the electrohydrodynamic heat pipe offers a number of advantages which must be weighed against its disadvantages in order to arrive at a proper assessment of its value in solving heat transfer problems. The fact that EHD devices are restricted to the relatively low performance organic dielectrics must be seen in light of a recognized need for heat pipes which operate in the moderate temperature range between those of water and the liquid metals. The greater complexity and attendant reliability problems of a high voltage system must be weighed against the benefits of direct on/off (and possibly continuous) heat flux control and 100% reliable priming. The questions raised by these issues are subjective and somewhat speculative in nature. They will probably remain unanswered until an EHD heat pipe is built and tested.

APPENDIX A

Performance Calculations for Optimized EHD Heat Pipes

Based on the procedure outlined in section IV.B, several EHD heat pipes of predetermined external specifications have been optimized by varying  $s$  and  $V$  to give maximum wick-limited (hydrodynamic) operation. Each optimization was carried out for a specific fluid and all pipes were specified to operate at the atmospheric boiling points of the fluid. Some of the results of these optimizing routines are plotted in Figure A1. Here are plotted predictions of maximum thermal throughput versus the EHD liquid transport factor from Eq. (32). For reference, each point is identified with the fluid used.

These results must be checked for their compatibility with evaporation and condensation heat transfer limits because the optimization itself is based purely on hydrodynamic considerations. A cursory examination of Figure A1 indicates that the predicted thermal throughputs of the larger diameter, axially shorter EHD heat pipes are not attainable without rather large total thermal potentials (temperature drop from the outside of the evaporator to the outside of the condenser). On the other hand, the longer models with small diameters promise to be able to transport significant heat and operate with acceptable  $\Delta T_c$ . Two such examples, with differing operating fluids and identical external dimensions, are considered here.

The heat pipes are of the form shown in Figure 3. The general physical specifications are:

length,	$L = 2. \text{ meters};$
diameter,	$D = 2.5 \text{ cm};$
electrode width,	$w = 1.0 \text{ cm};$
number of flow structures,	$n = 4,$
vessel thickness,	$\Delta x = 1/32'' \approx .079 \text{ cm (aluminum)}$

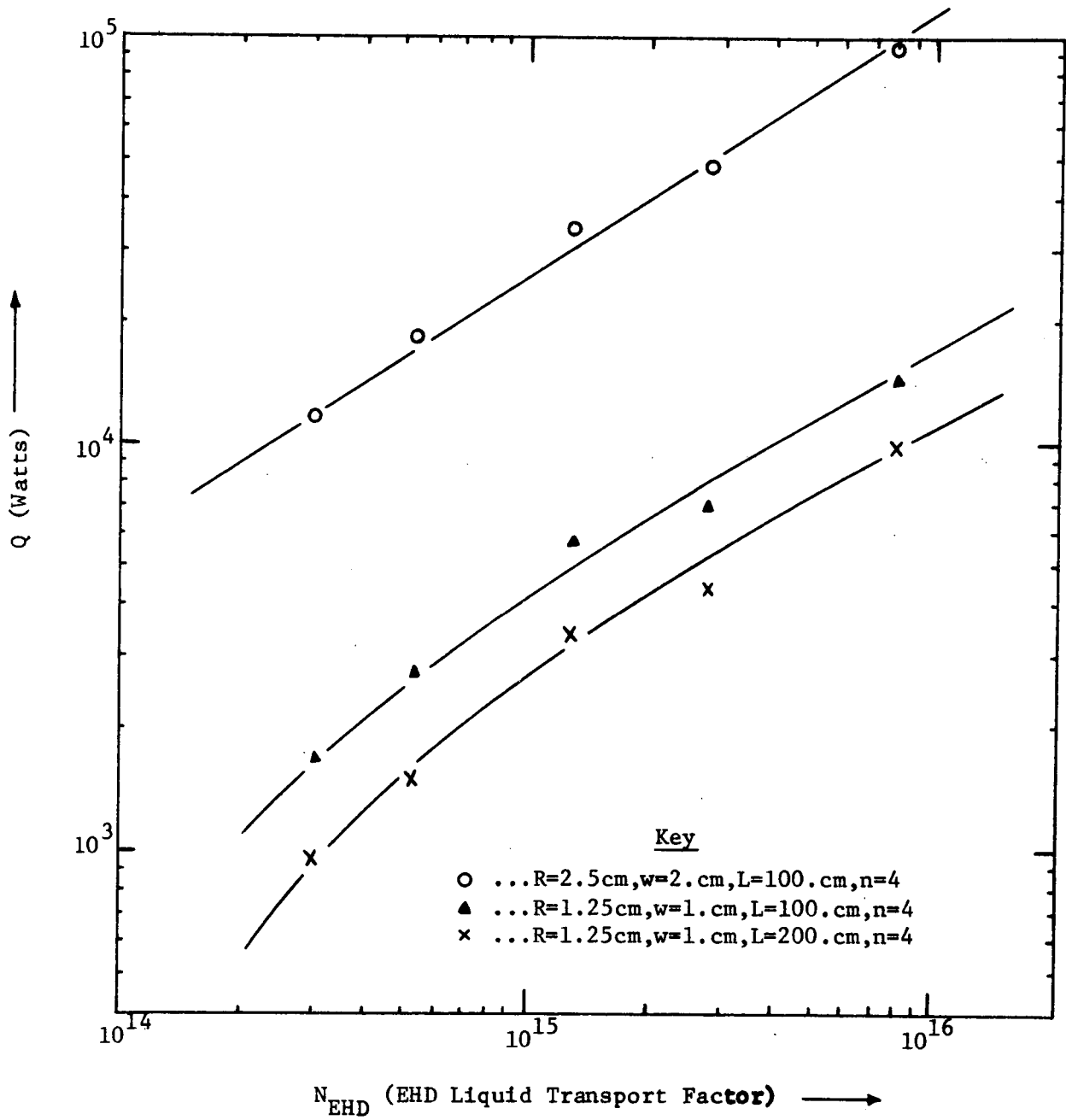


Figure A1. Theoretical Maximized Thermal Throughput versus  $N_{EHD}$  for several EHD Heat Pipes, in the Configuration of Fig. 3.

The working fluids chosen are Dupont Freon-113 (atmospheric boiling point  $T_b \approx 118^\circ\text{F}$ ), and Dow Dowtherm A ( $T_b \approx 495^\circ\text{F}$ ). It is further assumed that the inner walls of the heat pipes are threaded, to promote circumferential flow and the heat transfer processes at the evaporator and condenser. Experience with capillary artery-threaded groove heat pipes indicates that evaporation and condensation heat transfer coefficients are normally within 20% of each other;<sup>18</sup> thus, it is assumed here that the evaporator and condenser sections are of equal length (one meter each, with no adiabatic section). The calculations follow below:

<u>Freon-113</u>	<u>Dowtherm A</u>
optimized spacing $s = .16 \text{ cm}$	optimized spacing $s = .16 \text{ cm}$
optimized voltage $V = 25 \text{ Kv}$	optimized voltage $V = 33.8 \text{ Kv}$
operating @ 1 atmos.	operating @ 1 atmos.
$T_b = 118^\circ\text{F}$	$T_b = 495^\circ\text{F}$
(size and breakdown limited)	(size and breakdown limited)

Optimized Performance Parameters:

$Q = 3.40 \text{ KW}$	$Q = 9.76 \text{ KW}$
$\dot{m} = 23. \text{ grams/sec}$	$\dot{m} = 33. \text{ grams/sec}$
$v_\ell = 24. \frac{\text{cm}}{\text{sec}}, \text{ Re}_\ell = 1100.$	$v_\ell = 59. \frac{\text{cm}}{\text{sec}}, \text{ Re}_\ell = 3000.$
$v_v = 8.4 \frac{\text{m}}{\text{sec}}, \text{ Re}_v = 123,000$	$v_v = 22. \frac{\text{m}}{\text{sec}}, \text{ Re}_v = 186,000.$

Heat Transfer Considerations:

Assume  $\Delta T_{\text{evap}} \approx 10^\circ\text{F}$  &  $\Delta T_{\text{cond}} \approx 10^\circ\text{F}$  as reasonable design objectives for temperature control applications. Then, the needed heat transfer coefficients may be calculated.

	<u>Freon-113</u>		<u>Dowtherm A</u>
$\left. \begin{array}{l} h_{\text{evap.}} \\ \\ h_{\text{cond.}} \end{array} \right\}$	$\approx \frac{3.4 \cdot 10^3}{(10^2)(\pi)(2.5)(10)}$	$\left. \begin{array}{l} h_{\text{evap.}} \\ \\ h_{\text{cond.}} \end{array} \right\}$	$\approx \frac{9.76 \cdot 10^3}{(10^2)(\pi)(2.5)(10)}$
	$\approx .43 \frac{\text{watts}}{\text{cm}^2 \cdot ^\circ\text{F}}$		$\approx 1.24 \frac{\text{watts}}{\text{cm}^2 \cdot ^\circ\text{F}}$
or	$\approx 1370. \frac{\text{Btu}}{\text{hr-ft}^2 \cdot ^\circ\text{F}}$	or	$\approx 3940. \frac{\text{Btu}}{\text{hr-ft}^2 \cdot ^\circ\text{F}}$

Artery-threaded groove heat pipes have operated with up to

$\sim 2500. \frac{\text{Btu}}{\text{hr-ft}^2 \cdot ^\circ\text{F}}$  evaporator coefficients (+ 20% for the condenser),

using ammonia as the working fluid;<sup>18</sup> however, these heat pipes have not been optimized with respect to groove size or configuration. As stated in section III.C of this report, significantly higher heat transfer coefficients have been predicted by Bressler and Wyatt.<sup>28</sup> In particular, their analysis may be used to predict an evaporation coefficient of  $\sim 3. \frac{\text{watts}}{\text{cm}^2 \cdot ^\circ\text{F}}$  for Dupont

Freon-22<sup>®</sup> (a fluorinated hydrocarbon with properties quite similar to other Freons<sup>®</sup>, including Freon-113<sup>®</sup>). Note that the heat transfer coefficient required for the F-113 model is significantly lower than this value. No

prediction is available for Dowtherm A<sup>®</sup>, but the fluid's generally better heat transport properties would be expected to be reflected in it.

At present, a limited understanding of the evaporation and condensation heat transfer processes at grooved surfaces exists. Further, there is a lack of heat pipe data concerning groove optimization attempts. It is therefore not possible to judge whether the values of  $.43 \frac{\text{watts}}{\text{cm}^2 \cdot ^\circ\text{F}}$  for Freon-113 and  $1.24 \frac{\text{watts}}{\text{cm}^2 \cdot ^\circ\text{F}}$  for Dowtherm A are attainable. This must await further testing of artery-threaded groove devices with organic dielectric fluids. Another unanswered question is the quantitative extent of the effect of the electric field upon the coefficients.

In any case, it is of interest to assume that these coefficients are attainable, and to proceed with performance calculations.

(continued, Freon-113)	(Dowtherm A)
vapor expansion, $\Delta T_v = .22^\circ\text{F}$	vapor expansion, $\Delta T_v = 1.12^\circ\text{F}$
wall conductivity, $\Delta T_k = .6^\circ\text{F}$	wall conductivity, $\Delta T_k = .6^\circ\text{F}$

Total Thermal Potential:

$$T_t \approx 10 + 10 + .22 + .6$$

$$\approx 20.8^\circ\text{F}$$

$$T_t \approx 10 + 10 + 1.12 + .6$$

$$\approx 21.7^\circ\text{F}$$

Effective Thermal Transport:

$$QL_{\text{eff}} \approx (3.4 \cdot 10^3) (1)$$

$$\approx 3400. \text{ watt-meters}$$

$$\text{or} \approx 1.34 \cdot 10^5 \text{ watt-in.}$$

$$QL_{\text{eff}} \approx (9.76 \cdot 10^3) (1)$$

$$\approx 9760. \text{ watt-meters}$$

$$\text{or} \approx 3.85 \cdot 10^5 \text{ watt-in.}$$

(continued, Freon-113)

(Dowtherm A)

Effective Conductance:

$$\frac{Q}{\Delta T_t} \approx \frac{3.4 \cdot 10^3}{20.8}$$
$$\approx 163. \frac{\text{watts}}{^\circ\text{F}}$$

$$\frac{Q}{A_x \cdot \Delta T_t} \approx \frac{163.}{(\pi)(2.5)^2}$$
$$\approx 8.3 \frac{\text{watts}}{\text{cm}^2 \cdot ^\circ\text{F}}$$

or  $\approx 26,300 \frac{\text{Btu}}{\text{hr} \cdot \text{ft} \cdot ^\circ\text{F}}$

$$\frac{Q}{\Delta T_t} \approx \frac{9.76 \cdot 10^3}{21.7}$$
$$\approx 450 \frac{\text{watts}}{^\circ\text{F}}$$

$$\frac{Q}{A_x \cdot \Delta T_t} \approx \frac{450.}{(\pi)(2.5)^2}$$
$$\approx 23.0 \frac{\text{watts}}{\text{cm}^2 \cdot ^\circ\text{F}}$$

or  $\approx 73,000 \frac{\text{Btu}}{\text{hr} \cdot \text{ft} \cdot ^\circ\text{F}}$

The predicted performance parameters for these two EHD heat pipes indicate that these devices have a potential quite competitive to that of second generation artery threaded groove heat pipes presently being designed and tested. The validity of such conjecture is based upon successful resolution of the questions regarding heat transfer coefficients and fluid entrainment. Even if EHD heat pipes are found to require large thermal potentials in order to realize their high power capacities, they still should be of interest in many non-temperature control applications.

APPENDIX B

Nomenclature

A	=	area
E	=	electric field
$E_b$	=	breakdown field strength of vapor
f	=	fluid friction factor (dimensionless)
g	=	local gravitational acceleration
$g_o$	=	terrestrial gravitational acceleration (9.81 m/sec <sup>2</sup> )
h	=	liquid height of rise, also heat transfer coefficient
k	=	thermal conductivity
L	=	heat pipe length
$\dot{m}$	=	mass flow
N	=	fluid transport factor
n	=	# EHD flow structures in heat pipe
p	=	pressure
Q	=	thermal throughput
R	=	radius
Re	=	fluid Reynolds Number (dimensionless)
$r_1, r_2$	=	radii of curvature
$r_p$	=	pore radius
s	=	electrode spacing
$T_b$	=	liquid atmospheric boiling point (°F)
$T_n^e$	=	normal component of electric surface traction
V	=	voltage
v	=	velocity
$v_{EHD}$	=	EHD wave celerity
$We^E$	=	electric Weber Number (dimensionless)

w = electrode width  
 $\Delta x$  = heat pipe wall thickness  
 $\Delta$  = difference between quantities  
 $\gamma$  = surface tension  
 $\epsilon$  = dielectric constant  
 $\epsilon_0$  = permittivity of free space ( $8.85 \cdot 10^{-12}$  farads/meter)  
 $\theta$  = contact angle  
 $\lambda$  = latent heat of vaporization  
 $\mu$  = dynamic viscosity  
 $\rho$  = density  
 $\sigma$  = electrical conductivity  
 $\tau$  = surface shear  
 $\phi$  = angle of inclination of heat pipe

Subscripts:

a -- adiabatic  
cap -- capillary  
cond -- condenser  
EHD -- electrohydrodynamic  
eff -- effective  
evap -- evaporator  
k -- thermal conduction  
l -- liquid  
max -- maximum  
min -- minimum  
t -- total  
v -- vapor  
x -- axial cross section

REFERENCES

1. Abu-Romia, M. M., "Possible Application of Electro-Osmotic Flow Pumping in Heat Pipes", AIAA Paper #71-423, 6th Thermophysics Conf., Tullahoma, Tenn., April 26-28, 1971.
2. Melcher, J. R., Guttman, D. S., and Hurwitz, M., "Dielectrophoretic Orientation", J. Spacecraft and Rockets, vol. 6, no. 1, Jan. 1969, pp. 25-32.
3. Melcher, J. R., Hurwitz, M., and Fox, R. G., "Dielectrophoretic Liquid Expulsion", J. Spacecraft and Rockets, vol. 6, no. 9, Sept. 1969, pp. 961-7.
4. Lubin, B. T., and Hurwitz, M., "Vapor Pullthrough at a Tank Drain with and without Dielectrophoretic Baffling", Proc. of Conference on Long-Term Cryo-Propellant Storage in Space, NASA Marshall Space Flight Center, Huntsville, Ala., October, 1966.
5. Marco, S. M., and Velkoff, H. R., "Effect of Electrostatic Fields on Free-Convection Heat Transfer from Flat Plates", ASME Paper 63-HT-9, 1963.
6. Choi, H. Y-H., "Electrohydrodynamic Boiling Heat Transfer", Ph. D. Thesis, Department of Mechanical Engineering, Massachusetts Institute of Technology, Cambridge, Mass., January, 1962.
7. Bonjour, E., Verdier, J., and Weil, L., Chem. Eng. Progress, vol. 58, no. 7, July, 1962, pp. 63-66.
8. Markels, M., and Durfee, R. L., A. I. Ch. E. Journal, vol. 10, no. 1, Jan., 1964, pp. 106-110.
9. Asch, V., J. Applied Phys., vol. 37, no. 7, June, 1966, pp. 2654-8.

10. Choi, H. Y-H., "Electrohydrodynamic Condensation Heat Transfer",  
ASME Paper 67-HT-39, J. Heat Transfer, vol. 90, series C, No. 1,  
Feb., 1968, pp. 98-102.
11. Holmes, R. E., "Condensation of a Dielectric Vapor in the Presence of  
a Non-Uniform Electric Field", Ph. D. Thesis, Department of  
Mechanical Engineering, Rice Univ., Houston, Texas, 1967.
12. Holmes, R. E., and Chapman, A. J., "Condensation of Freon-114 in the  
Presence of a Strong, Nonuniform, Alternating Electric Field,"  
ASME Paper # 70-HT-6, J. Heat Transfer, vol. 92-C, no. 4, November,  
1970, pp. 616-620.
13. Holmes, R. E., and Anno, J. N., "An Electrofluid-Dynamic Cooling  
System Concept for Spacecraft Environmental Control", ASME  
Paper 70-HT/Spt-24, Space Technology and Heat Transfer Conference,  
Los Angeles, June 21-24, 1970.
14. Jones, T. B., "Dynamics of Electromechanical Flow Structures",  
Ph. D. Thesis, Department of Electrical Engineering, Massachusetts  
Institute of Technology, Cambridge, Mass., August, 1970.
15. Basiulis, A., and Filler, M., "Operating Characteristics and Long  
Life Capabilities of Organic Fluid Heat Pipes", AIAA Paper # 71-408,  
6th Thermophysics Conf., Tullahoma, Tenn., April 26-28, 1971.
16. Marcus, B. D., "Theory and Design of Variable Conductance Heat Pipes:  
Hydrodynamics and Heat Transfer", Research Report #1, NASA Contract  
# NAS 2-5503, TRW Systems, Redondo Beach, California, April, 1971.
17. Stratton, J. A., Electromagnetic Theory, Chapter 11, McGraw-Hill,  
New York, 1941.
18. Marcus, B. D., TRW Systems, Redondo Beach, California, September, 1971,  
private communication.

19. Feldman, K. T., "Analysis and Design of Heat Pipes", Bureau of Engineering Research, University of New Mexico, Albuquerque, New Mexico, June, 1970.
20. Rouse, H., Fluid Mechanics for Hydraulic Engineers, section 59, Dover Publications, New York, 1961.
21. Cotter, T. P., Theory of Heat Pipes, Los Alamos Scientific Laboratory, Report # LA-3246-MS, February, 1965.
22. Rohsenow, W. M., and Choi, H. Y-H., Heat, Mass, and Momentum Transfer, Prentice-Hall, Englewood Cliffs, N. J., 1961.
23. Kirkpatrick, J. P., NASA Ames Research Center, Moffett Field, California, September, 1971, private communication.
24. Armstrong, R. J., Evaporative Cooling with Freon<sup>®</sup> Dielectric Liquids, Dupont Freon Technical Bulletin # EL-11, Wilmington, Delaware, 1966.
25. Moritz, K., "Ein Wärmerohr neuer Bauart das Gewinde-Arterien-Wärmerohr", Chemie-Ingenieur Technik, vol. 41, no. 1-2, January, 1969, pp. 37-40.
26. Bienert, W., and Kroliczek, E., "Experimental High Performance Heat Pipes for the OAO-C Spacecraft", ASME Paper # 71-Av-26, presented at SAE/ASME/AIAA Life Support and Environmental Control Conf., July 12-14, 1971, San Francisco, Cal.
27. Moritz, K., "Zum Einfluss der Kapillargeometrie auf die maximale Heizflächenbelastung in Wärmerohren", doctoral dissertation, University of Stuttgart, Germany, 1969.
28. Bressler, R. G., and Wyatt, P. W., "Surface Wetting Through Capillary Grooves", ASME Paper # 69-HT-19, J. Heat Transfer, vol. 92-C, no. 1, February, 1970, pp. 126-132.

29. Marcus, B. D., "Theory and Design of Variable Conductance Heat Pipes: Control Techniques", Research Report #2, NASA Contract # NAS 2-5503, TRW Systems, Redondo Beach, California, July, 1971.